Editors' Suggestion

Colloidal gelation induced by ring polymers

Esmaeel Moghimi,[1,2] Iurii Chubak,[3,4] Maria Kaliva,[1,2] Parvin Kiany,[1,2] Taihyun Chang,[5] Junyoung Ahn,[5] Nikolaos Patelis,[6] Georgios Sakellariou,[6] Sergei A. Egorov,[7,8] Dimitris Vlassopoulos,[1,2] and Christos N. Likos[3]

[1]*FORTH, Institute of Electronic Structure and Laser, 70013 Heraklion, Crete, Greece*

[2]*Department of Materials Science and Technology, University of Crete, 70013 Heraklion, Crete, Greece*

[3]*Faculty of Physics, University of Vienna, Boltzmanngasse 5, 1090 Vienna, Austria*

[4]*Physico-Chimie des Électrolytes et Nanosystèmes Interfaciaux, Sorbonne Université CNRS, F-75005 Paris, France*

[5]*Division of Advanced Materials Science and Department of Chemistry, Pohang University of Science and Technology, Pohang 37673, Korea*

[6]*Department of Chemistry, National and Kapodistrian University of Athens, 15771 Athens, Greece*

[7]*Department of Chemistry, University of Virginia, Charlottesville, Virginia 22901, USA*

[8]*The Erwin Schrödinger International Institute for Mathematics and Physics, Boltzmanngasse 9, 1090 Vienna, Austria*

(Received 19 September 2023; revised 23 November 2023; accepted 4 January 2024; published 22 January 2024)

We provide unambiguous experimental evidence that ring polymers are stronger depleting agents in colloidal suspensions than their linear counterparts. We use an intermediate volume fraction ($\phi_c = 0.44$) colloidal gel based on the classic poly(methyl methacrylate) (PMMA) hard spheres, in which the polystyrene depletant is either linear or ring of the same molar mass or the same size. We systematically increase the depletant concentration from zero (no attraction) to well above the gelation point and find that in the presence of rings, gels are formed at smaller concentrations and possess a larger storage modulus in comparison to those induced by the linear chains. Consequently, the yield stress is enhanced; however, the yield strain (gel deformability) remains concomitantly unaffected. Our experimental findings are in agreement with theoretical calculations based on effective interaction potentials. Hence, polymer architecture is a powerful entropic tool to tailor the strength of colloidal gels.

DOI: 10.1103/PhysRevResearch.6.013079

I. INTRODUCTION

Control over the range and strength of the attractive interactions between colloidal particles is a problem of fundamental importance for metastable materials, and critical for the design of such materials for specific applications. It allows for the steering of phase transitions [1], the stabilization of finite clusters of various morphologies [2–4], as well as the formation of different types of glasses [5–7] and gels [8,9]. The addition of nonadsorbing polymer in a colloidal suspension induces a depletion attraction of tunable range and strength between the colloids [10]. Accordingly, the study of depletion interactions is a central problem in statistical physics, bearing great relevance not only in the fundamental sense mentioned above, but also in a wide range of applications: examples include flocculation of impurities in water treatment, aggregation of DNA and crystallization of proteins [11], and properties of many consumer products, such as paints, foods, and pharmaceuticals [12]. Essential in understanding these phenomena are two ingredients: interactions between depletants and interactions of depletants with solid particles. Nonadsorbing linear-polymer chains have been used routinely as depletant agents; in this case, the strength and range of depletion potential between particles are adjusted by the concentration and size of the depletant, respectively [13,14]. Less attention has been paid to the role of macromolecular architecture of the depletant [15–18]. Further, a recent theoretical study has indicated that ring polymers exhibit a stronger depletion force near a wall compared to linear chains [19,20]. When a ring polymer is brought near a solid wall (or, equivalently, a hard sphere particle of much larger size) or is confined between two walls (or, equivalently, two large hard-sphere particles), its configuration is drastically affected, and for strong confinements it changes from three dimensional to two dimensional, which significantly reduces its entropy. The effective interaction between the center of mass of a ring polymer and a planar impenetrable wall yields much higher interaction energies in comparison to the case of linear chains. Unlike linear chains, rings in contact with one and two hard walls in the dilute solution exhibit an oscillatory density profile, reminiscent of hard-sphere systems. The corresponding depletion potential also preserves this oscillatory shape, in sharp contrast to linear polymers [19,20].

Despite the above developments and the potential of ring architecture to strengthen gels, an experimental and theoretical investigation of the impact of ring topology on the depletion interactions in colloidal suspensions of hard particles and of the influence ring polymers have on the rheology of dense colloidal suspensions is lacking. Yet, it is much needed as tailoring depletion interactions at the molecular

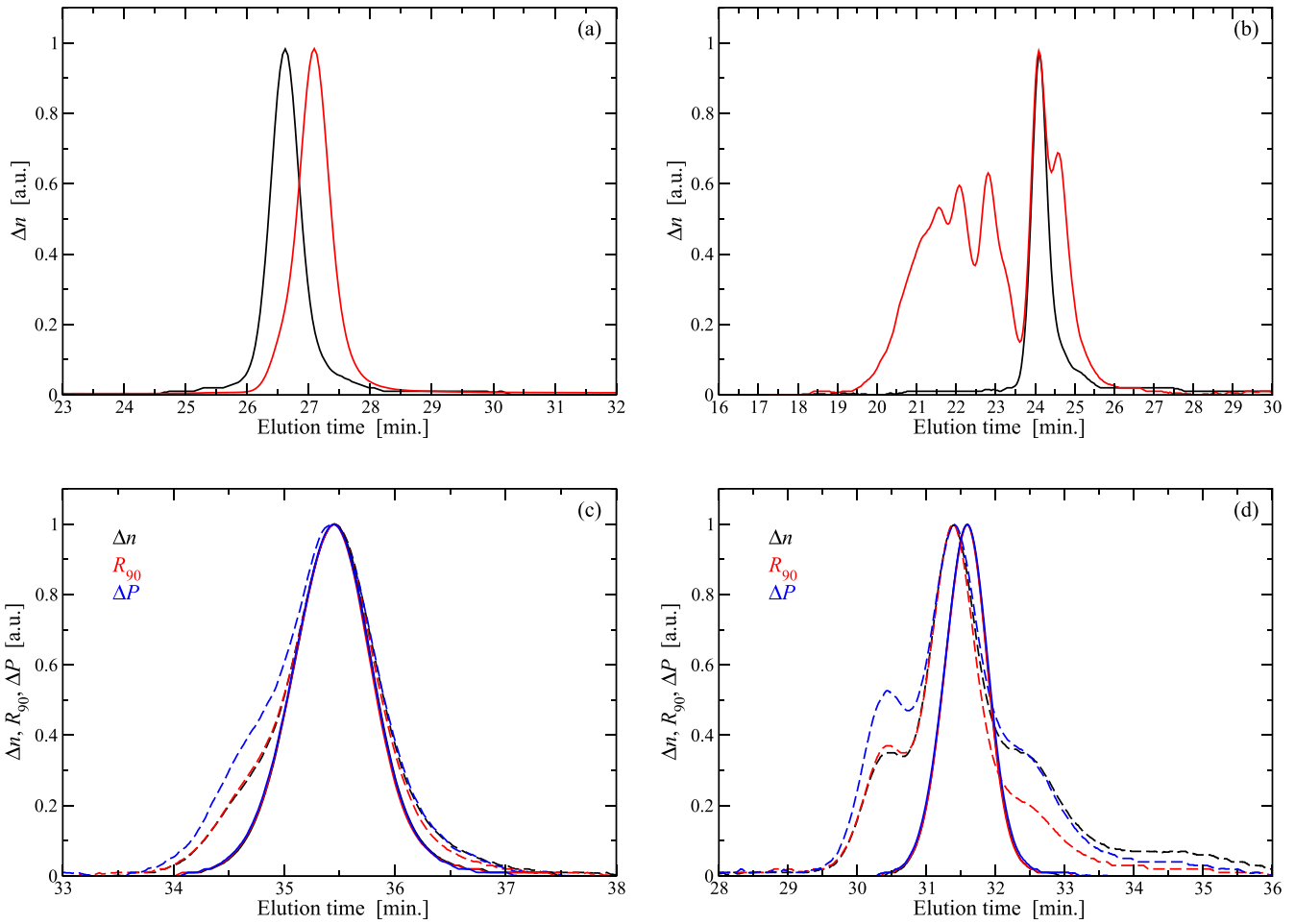

FIG. 1. (a) Size exclusion chromatography (SEC) chromatogram of the linear precursor Linear-50 (black solid line) and Ring-50 (red solid line) after purification by fractional precipitation in methanol. (b) SEC chromatogram of linear precursor Linear-160 (black solid line) and Ring-160 (red solid line) as prepared, prior to purification. The SEC system was equipped with four PLgel mixed C columns and THF was used as an eluent at flow rate 1 mL/min. (c) SEC-triplet detection chromatogram of Ring-50 after fractional precipitation (dashed line) and after purification by liquid chromatography at the critical condition (LCCC) (solid line). (d) SEC-triplet detection chromatogram of Ring-160 after fractional precipitation (dashed line) and after purification by liquid chromatography at the critical condition (LCCC) (solid line). The SEC system was equipped with three columns and THF was used as an eluent at a flow rate of 0.7 mL/min.

level is a formidable scientific challenge of prime technological significance. In this paper, we address this challenge by combining experiments with theoretical predictions. We investigate a colloidal gel in which the depletant is either ring or linear chain of the same molar mass or the same size. Our results indicate that in the presence of rings, gelation takes place at smaller polymer concentrations. Gels with ring depletants are much stronger and have a higher yield stress while their yield strain is unaffected, compared to the case of linear additives. These findings hallmark the importance of polymer architecture on the depletion potential and hence advance our understanding of the physics of colloidal interactions. At the same time, they pave the way for designing gels of varying strength via macromolecular architecture, while keeping the same chemistry, particle fraction, and size ratio.

The rest of the paper is organized as follows: In Sec. II, we describe the materials, the polymer synthesis, and the applied rheological methods, and in Sec. III, we present our experimental results from rheology. In Sec. IV, we describe the coarse-graining process that lies at the basis of our theoretical approach. The depletion potentials are presented in Sec. V and the resulting phase diagram in Sec. VI. Finally, in Sec. VII, we draw our conclusions, whereas we delegate some results on gelation using star polymer as depletants to the Appendix, for comparison with the ring- and linear-polymer induced gels.

II. MATERIALS AND METHODS

Polystyrene ring samples Ring-50 and Ring-160 as well as the linear polystyrene precursor Linear-50 have been synthesized using anionic methods, as described previously [21,22]. Briefly, Linear-50 was synthesized using potassium naphthalenide as the initiator in tetrahydrofuran (THF), while cyclic Ring-50 and Ring-160 were prepared by coupling the di-anionic linear precursor Linear-50 and Linear-160 with α, α' dibromo-p-xylene in very dilute THF solution. The characterization of the linear samples by size exclusion chromatography (SEC) is depicted in Figs. 1(a) and 1(b). All ring samples were first purified by fractional precipitation in methanol [22], followed by

TABLE I. The polydispersities M_w/M_n of the polymers employed in this work.

Sample	M_w/M_n
Ring-50	1.002[a]
Linear-50	1.14
Linear-10	1.14
Ring-160	1.002
Linear-73	1.11
Star, $f = 32$	1.14
Star, $f = 34$	1.13

[a]After critical fractionation.

further purification by liquid chromatography at the critical conditions (LCCC) to remove any traces of the linear precursors [23–25]; see Figs. 1(c) and 1(d). The weighted-average molar mass was determined by SEC and found to be 160 kg/mol for Linear-160 and Ring-160 and 50 kg/mol for Linear-50 and Ring-50. The polydispersity M_w/M_n measured by SEC was below 1.08 for all samples, as shown in Table I. We used poly(methyl methacrylate) (PMMA) particles, sterically stabilized by a short layer ($\cong$ 10 nm) of grafted poly(hydrostearic acid) (PHSA) chains. They were dispersed in dioctyl phthalate (DOP), a high boiling point (385 °C) solvent to avoid evaporation [26–28]. We performed experiments with two sets of colloidal particles with hydrodynamic radii $R_c = 132$ and 89 nm (measured in a dilute solution by dynamic light scattering). Depletion attractions were introduced by adding anionically synthesized, well-characterized, nonadsorbing linear and ring polystyrene (PS) with different molar masses M_w and hydrodynamic radii R_H, shown in Table II. We further introduce the size ratio $q \equiv R_H/R_c$ between the polymer and the colloid, which is shown in the last column of Table II. The gel was prepared at an intermediate colloid volume fraction, $\phi_c = 0.44$, and different polymer concentrations.

Rheological measurements were performed with an ARES-HR (100-FRTN1) sensitive strain controlled rheometer (TA Instruments, USA) equipped with a force balance transducer. We used a homemade stainless-steel cone-plate geometry of diameter 8 mm, cone angle of 2.6°, and truncation of 0.045 mm, with a roughness of a few-hundred microns (except for the smooth region near the truncation), which inhibited slip at the wall [29]. The temperature was set to

TABLE II. Sample parameters. Columns from the left show the sample code, the weighted-average polymer molar mass M_w, the respective number of Kuhn segments, N, the overlap concentration c^*, the hydrodynamic radii R_H of the polymers and R_c of the colloidal particles, as well as the size ratio $q \equiv R_H/R_c$.

Sample	M_w (kg/mol)	N	c^* (g/ml)	R_H (nm)	R_c (nm)	q
Ring-50	48	70	0.530	3.3	132	0.025
Linear-50	46	70	0.093	5.8	132	0.044
Linear-10	10	14	0.226	2.6	132	0.02
Ring-160	160	222	0.124	8	89	0.09
Linear-73	73	101	0.056	8	89	0.09

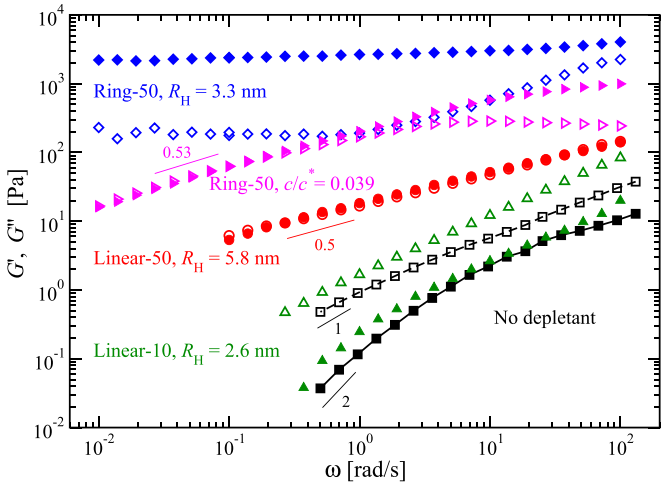

FIG. 2. Linear viscoelastic spectra depicting the storage G' (closed symbols) and loss G'' (open symbols) moduli as a function of the angular frequency ω at a strain amplitude of 0.05%, for a PMMA colloidal dispersion in DOP with $\phi_c = 0.44$, $R_c = 132$ nm and different PS depletants marked on the plot. For all samples with nonzero depletant, $c/c^* = 0.12$; for the right-pointing triangles system, $c/c^* = 0.039$.

$T = 30$ °C using a standard Peltier plate, corresponding to good solvent conditions for the present system. In order to erase loading history effects, before each experiment the sample was presheared at a shear rate of $\dot{\gamma} = 200\ s^{-1}$ for 100 s, which produced reproducible results. Visual observations confirmed that the sample was intact during preshearing. Subsequently, the flow was stopped and the sample was allowed to age until constant values of the linear viscoelastic moduli were reached. Finally, small amplitude oscillatory shear measurements, typically lasting 1 hour, were performed with strain amplitude of 0.05% over a maximum frequency range of 100–0.01 rad/s, to probe the linear viscoelastic spectrum. The limit of the linear viscoelastic (LVE) regime was determined with dynamic strain sweep experiments at various frequencies.

III. RHEOLOGICAL EXPERIMENTS

The elasticity of colloidal gels serves as a measure of depletion forces acting on the colloidal particles [30]. Here we focus on determining the LVE response of the gels. In Fig. 2, we show the LVE spectrum of a PMMA colloidal dispersion with PS depletant concentration of $c/c^* = 0.12$, where c^* is the overlapping concentration in DOP (c/c^* is actually an effective volume fraction based on R_H). The corresponding spectra for $c/c^* = 0.35$ are shown in Fig. 3. The results are compared for a ring polymer and its linear counterpart at both the same M_w and nearly the same R_H (nearly the same volume fraction for the two polymer architectures). The dispersion without depletant is a viscoelastic liquid characterized by values of loss modulus G'' exceeding the respective storage modulus G' and terminal flow scaling $G' \sim \omega^2$, $G'' \sim \omega$. Adding a low molar mass linear PS depletant ($M_w = 10$ kg/mol) with very similar size as the ring leads to a weak increase of both

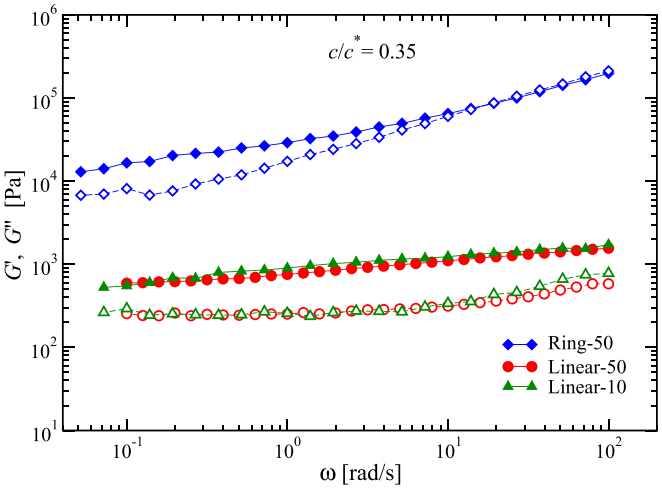

FIG. 3. Linear viscoelastic spectra depicting the storage G' (closed symbols) and loss G'' (open symbols) moduli as a function of the angular frequency ω at a strain amplitude of 0.05%, for a PMMA colloidal dispersion in DOP with $\phi_c = 0.44$, $R_c = 132$ nm and different PS depletants, marked on the legend, with $c/c^* = 0.35$.

moduli; however, the overall response remains liquidlike. On the other hand, in the presence of a larger linear depletant ($M_w = 50$ kg/mol), a critical gel is formed where the moduli collapse onto each other and decay with the slope of 0.5. In stark contrast, rings with the same $M_w = 50$ kg/mol yield a strong gel marked by $G' > G''$ and G' independent of frequency over the entire range of examined frequencies and exceeding that of the PMMA suspension by 2.5 to 4.5 decades. The corresponding critical gel induced by the ring polymers is formed at a much lower $c/c^* \cong 0.039$, as can be seen in Figs. 2 and 4.

In Fig. 5 we examine the effect of the depletant's effective volume fraction on gel strength by plotting G' at $\omega = 1$ rad/s over a broad range of c/c^*, from zero (no attraction) to well above the onset of gelation. The choice of ω is somewhat arbitrary and based on the fact that this is the lowest frequency for which the data for all depletants are available; the same

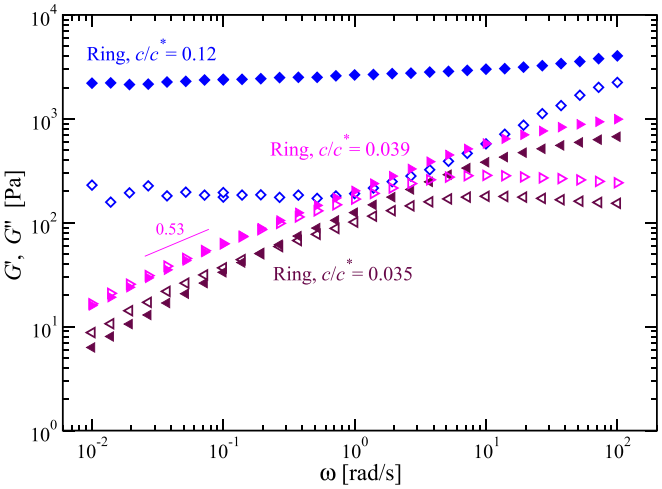

FIG. 4. Linear viscoelastic spectra of three colloid-ring mixtures at three different values of c/c^* of the rings, as indicated in the plot.

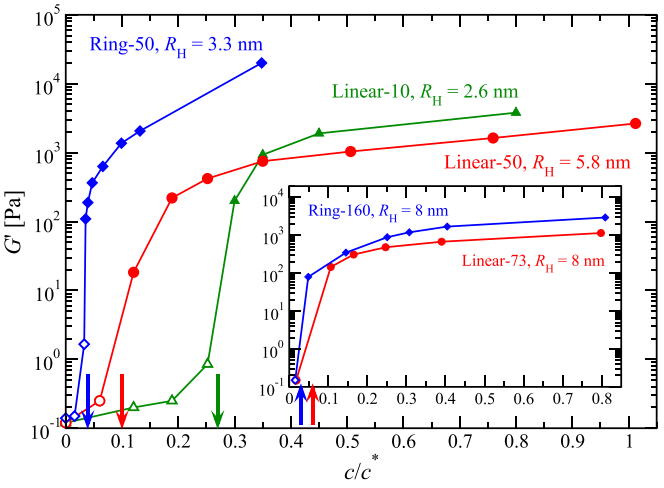

FIG. 5. Storage modulus G' at frequency $\omega = 1$ rad/s as a function of the depletants' effective volume fraction, for various depletants shown in the legend. Data refer to the PMMA colloidal dispersion of Fig. 2. The size ratio for the ring is $q = 0.025$ and for the linear is $q = 0.02$ ($M_w = 10$ kg/mol) or $q = 0.044$ ($M_w = 50$ kg/mol). Empty symbols are data below gelation ($G' < G''$), whereas filled symbols are data above gelation ($G' \geqslant G''$). Inset: Same representation as in the main panel, but with smaller particle size $R_c = 89$ nm and a larger size ratio, $q = 0.09$. The inset axes have the same labels as those of the main plot. The thick vertical arrows in the main plot and in the inset mark the onset of gelation for the corresponding depletant, color matched to the curves on the panels.

qualitative conclusions can be drawn for other frequencies. The onset of gelation is usually determined as the point in which the tangent of the phase difference δ between G' and G'' reaches unity [31]. Here, we follow a more simplistic definition of the onset of gelation and assign it to the midpoint between the highest value of c/c^* at which the sample is fluid and the lowest value of c/c^* at which the sample is solid. This is adequate since we focus on the qualitative aspects of the effect.

As expected, an increase in depletant concentration leads to an increase in G' due to particle clustering. G' increases abruptly when gelation takes place ($G' \geqslant G''$). Within the gel regime, G' grows weakly, following the increase of interparticle depletion forces with c/c^* [32]. Over the entire range of concentrations, the ring-polymer depletant forms a stronger gel, manifested by a larger value of G' (see, also, Fig. 2), indicating a stronger depletion force compared to the case of a linear-polymer depletant with the same molar mass or nearly the same size. Moreover, in the presence of rings, gelation takes place at lower values of c/c^*, as denoted by the vertical arrows in Fig. 5. Note that inside the gel region, G' increases linearly with depletant concentration, which is the case for both linear depletants of molecular mass 10 and 50 kg/mol, consistent with literature [33], but not for rings: the latter exhibit a linear increase for $c/c^* \leqslant 0.13$ and then a sharp increase for $c/c^* > 0.13$. Of course, the present results refer to a specific frequency, as already mentioned.

To address the role of the size ratio, in the inset of Fig. 5, we compare the effects of ring- and linear-polymer depletants of the same size, at a larger $q = 0.09$. The picture is

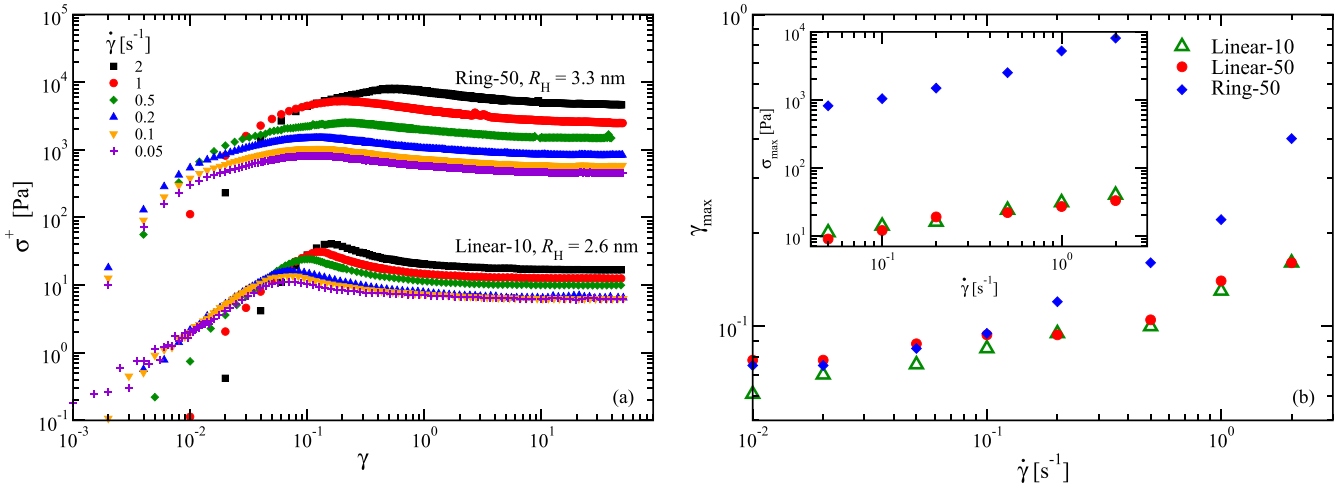

FIG. 6. (a) Shear stress growth function obtained from start-up shear flow from experiments performed at different shear rates, as shown in the legend, for two colloidal gels ($\phi_c = 0.44$, $R_c = 132$ nm) based on linear- and ring-polymer depletants with nearly the same size at an effective volume fraction of $c/c^* = 0.35$. (b) The respective yield strain (main plot) and yield stress (inset) values as functions of the shear rate.

qualitatively unchanged, i.e., the gel from rings is stronger compared to that from their linear counterpart with the same size. Quantitatively, it can be seen that for given c/c^*, the smaller-q depletants are more effective in strengthening the elasticity of the gel, a feature that can be understood in terms of the q dependence of the depth of the contact value of the depletion potential, $\beta W(r)$, between the two colloids, where $\beta = (k_B T)^{-1}$, with Boltzmann's constant k_B and the absolute temperature T. The latter depends on the osmotic pressure Π_p of the polymers and on the overlap volume V_o of the depletion regions as $\beta W(2R_c) = -\Pi_p V_o$ [34]. At fixed c/c^*, the ideal contribution to the former, which is dominant at low c/c^* values, scales as $\Pi_p \sim q^{-3}$, while $V_o \sim q^2$, resulting in an overall $\beta W(2R_c) \sim q^{-1}$ dependence. On the other hand, at $q = 0.09$, the difference in elasticity between ring-based and linear-based gels is much smaller compared to the smaller value $q = 0.025$, as can be seen in Fig. 5. This effect may be due to the fact that the small size-ratio polymers have a small number of effective Kuhn lengths and, therefore, specific, rigidity-related effects probably play a role. In particular, rigidity further enhances the entropy loss of a semiflexible ring close to a colloidal particle with respect to that of a linear chain, thus leading to a further strengthening of the attractive, effective colloid-colloid forces in a ring solution.

We put the experimental findings on the strengthening of the colloidal gel through addition of ring-polymer depletants in a broader context by examining the effects of star architecture on gel elasticity, and we present the results in the Appendix. There we show that the effect of the ring polymer is quantitatively very similar to that of the addition of 64-arm star polymers at the same values of c/c^* and stronger than that of 32-arm stars; see Fig. 11 below. This is a quite unexpected result, as the star architecture is very different from that of a ring. Indeed, the former is a soft colloid at the intermediate regime between a polymer chain and a hard sphere [35], whereas the latter is obtained from a linear chain through closure of its two ends; yet, the depletion effects of the ring are much more similar to those of a star than to those of a linear chain. The above combination of results points to the crucial role played by the macromolecular architecture on the properties of colloidal gels.

To explore the consequences of enhanced gelation due to rings on the nonlinear response of the mixtures, we compare the gels during start-up shear flow. The sample was subjected to a constant shear rate, and the dependence of the shear stress growth function (transient stress) on the accumulated strain was probed. Representative data are depicted in Fig. 6(a) for gels from ring and linear depletants of nearly the same size. The initial growth is followed by an overshoot, marking the onset of yielding, and eventually a steady state at large strain values. The extracted yield strain is depicted in the main panel and the yield stress is depicted in the inset of Fig. 6(b), which increase with shear rate, as expected for an activated process and reflect the breakage of bonds [36]. The ring has a clear impact on increasing the yield strain at large values of shear rate (by a factor of two for $\dot{\gamma} > 1$ s^{-1}), and substantially increasing the yield stress (by more than two orders of magnitude), reflecting the stiffening of the network with an accompanied enhanced deformability, a rather unique and highly desirable material behavior [37].

The large enhancement of yield stress in the case of ring depletants can be understood by approximating the relation between yield stress σ_y and yeild strain γ_y as $\sigma_y \approx G_p \gamma_y$, where G_p is the low-frequency plateau modulus. With the yield strain being virtually identical for linear and ring depletants at low rates, the yield stress increase reflects an increase of G_p by a

TABLE III. Fitting parameters for the ring-ring potentials in Eq. (1).

N	U_0	$\frac{R_<}{R_g^{ring}}$	$\frac{R_>}{R_g^{ring}}$
100	2.3791	0.8398	1.2838
200	1.9871	0.8609	1.2809
400	1.8063	0.8725	1.2792

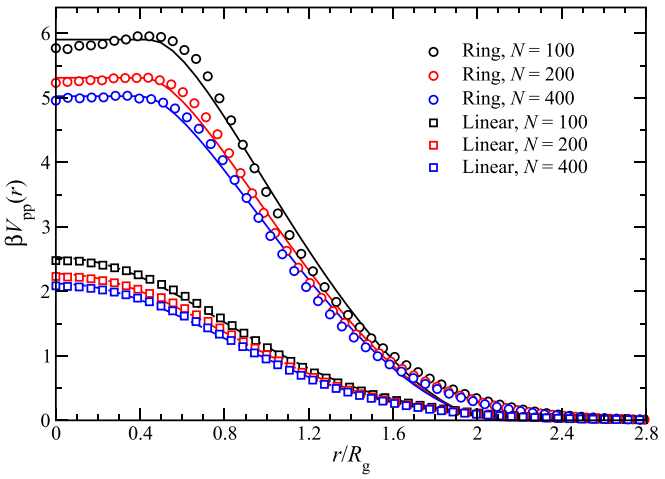

FIG. 7. Effective potentials $V_{pp}(r)$ between the centers of mass of polymers of degrees of polymerization N. Circles refer ro ring polymers and squares to linear ones. The lines are fits with functional forms described in the text.

factor of about 30, as shown in Fig. 3. In addition, different depletants (rings and linear chains) with the same shear history (leading to reproducible rheology in each case) may affect the microstructure of the depletion gel differently (this is a subject of future work). This is also implied by the different dependence of the storage modulus on concentration discussed above. Therefore, the plateau modulus and microstructural changes are responsible for the different values of yield stress.

IV. COARSE GRAINING OF THE COLLOID-POLYMER MIXTURES: EFFECTIVE INTERACTIONS

We employed computer simulations to derive the effective potentials $V_{pp}(r)$ between the centers of mass of the polymers and $V_{cp}(r)$ between the center of the colloid and the center of mass of the polymer. Both the polymer model and the method for measuring the effective interactions are described in Refs. [19,38]. Three different polymers with monomer numbers $N = 100$, 200, and 400 have been employed to check whether the scaling limit has been reached.

The ring-ring effective potentials are shown in Fig. 7 and can be accurately modeled by the following expression [39]:

$$\beta V_{pp}^{ring}(r) = \frac{U_0}{\left(R_g^{ring}\right)^3} \begin{cases} \frac{4\pi}{3} R_<^3 & \text{for } 0 \leqslant r < R_- \\ \frac{\pi}{12r}(r^2 + 2R_+ r - 3R_-^2)(R_+ - r)^2 & \text{for } R_- \leqslant r < R_+ \\ 0 & \text{for } r \geqslant R_+, \end{cases} \tag{1}$$

where $R_\pm = R_> \pm R_<$, whereas $R_>, R_<$, and V_0 are optimization parameters. The values of the best-fit parameters are summarized in Table III for pairs of rings of the same length N, with $N = 100, 200$, and 400, that have gyration radii $R_g^{ring}/\sigma = 5.512, 8.417$, and 12.772, respectively, for the employed microscopic model with monomer size σ. In Fig. 7, we also show effective potentials between two linear polymers of the lengths N with $N = 100, 200$, and 400 and sizes $R_g^{linear}/\sigma = 7.572, 11.594$, and 17.646, respectively. The effective potentials in Fig. 7 can be accurately modeled with a Gaussian,

$$\beta V_{pp}^{linear}(r) = V_0 \exp(-\alpha r^2), \tag{2}$$

where r is measured in units of R_g^{linear}. The values of the best-fit parameters are summarized in Table IV. The interactions between a ring/linear polymer and a colloid have been derived using a Widom insertion algorithm and equilibrium ring configurations. The potentials between the center of mass of a polymer and a colloid of radius $R_c = R_g/q$ are plotted in Fig. 8 for rings (left column) and linear chains (right column).

TABLE IV. Fitting parameters for the linear-linear potentials in Eq. (2).

N	V_0	$\alpha(R_g^{linear})^2$
100	2.5254	0.7946
200	2.2730	0.7962
400	2.1204	0.7989

For colloid-polymer separations $r \geqslant R_c$, the respective potentials can be quite reasonably described by a fit of the form [19,40,41]

$$\beta V_{cp}(r) = A \exp\left(-B\Delta_s - C\Delta_s^2 - D\Delta_s^3\right), \tag{3}$$

where $\Delta_s \equiv s - S_c$, $s \equiv r/R_g$ is the distance from the surface of the colloid measured in units of $R_g^{ring/linear}$, and $S_c \equiv R_c/R_g$. The best-fit parameters are listed in Table V for rings and in Table VI for linear chains.

V. THE DEPLETION POTENTIAL: DENSITY FUNCTIONAL THEORY

The theoretical approach is based on the coarse-grained approach of the preceding section, thereby introducing a binary mixture of colloids (c) and polymers (p) and their effective interactions $V_{cc}(r)$, $V_{cp}(r)$, and $V_{pp}(r)$. The bare interaction $V_{cc}(r)$ between the centers of the two colloids at separation r is of a hard sphere with diameter $2R_c$,

$$V_{cc}(r) = \begin{cases} \infty, & r \leqslant 2R_c \\ 0, & r > 2R_c. \end{cases} \tag{4}$$

The effective interaction potential between two colloids in a polymer solution, $\Phi_{cc}(r)$, is the sum of the bare colloid-colloid pair potential, $V_{cc}(r)$, and the polymer-mediated depletion interaction $W(r)$,

$$\Phi_{cc}(r) = V_{cc}(r) + W(r). \tag{5}$$

To derive the polymer-induced depletion interaction $W(r)$ between the colloids, we consider two spherical colloidal

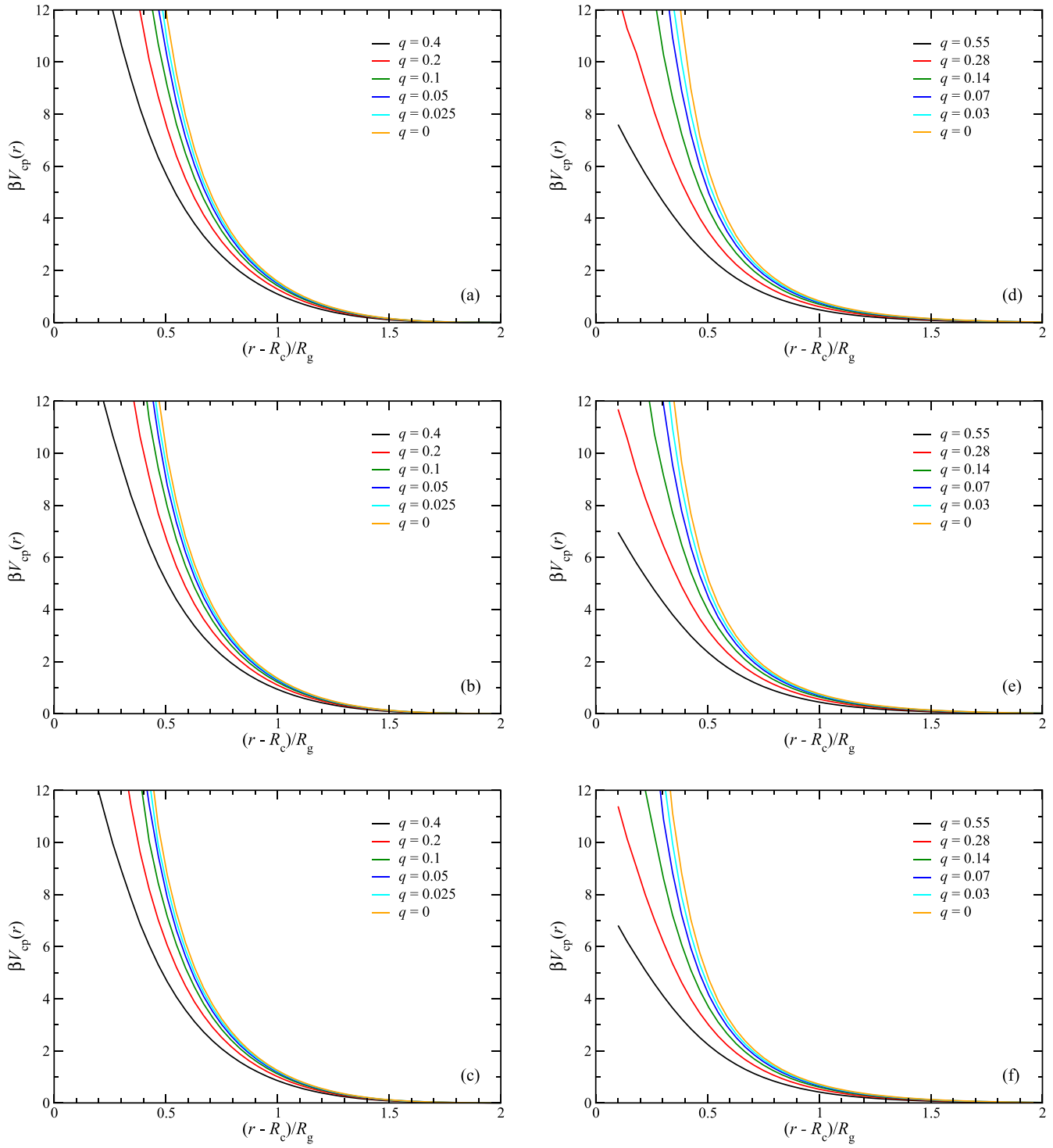

FIG. 8. The effective potentials $V_{cp}(r)$ acting between the center of mass of a polymer of gyration radius R_g and a colloid of radius R_c, expressed as a function of the distance of closest approach between the center of mass of the polymer and the surface of the colloid, $r - R_c$, in R_g units. The size ratios are indicated in the legends, with $q = 0$ representing a flat wall. (a)–(c) Ring polymers; (d)–(f) linear polymers. In each column, the degrees of polymerization of the polymers employed in the simulation are $N = 400$, 200, and 100, from top to bottom.

particles of radius R_c, one fixed at the origin and another at $\mathbf{r}$, immersed in a solvent composed of depletants, i.e., either linear or ring polymers. The two fixed colloidal particles act as an external potential on the polymer solution. The depletion interaction $W(r)$ is calculated employing a classical density functional theory (DFT) approach, from which the equilibrium polymer density profile $\rho(\mathbf{x};\mathbf{r})$ is obtained, where $\mathbf{x}$ denotes an arbitrary position in space and $\mathbf{r}$ the parametric dependence of the profile on the vector separating the two colloidal particles. The starting point of the DFT treatment is the expression of the grand potential $\Omega[\rho]$ as a functional of $\rho(\mathbf{x};\mathbf{r})$. Minimization of $\Omega[\rho]$ with respect to the latter yields

TABLE V. Fitting parameters for the ring polymer-colloid effective interactions of Eq. (3), for rings of different length N and size ratio q.

$N=100$	$q=0.4$	$q=0.2$	$q=0.1$	$q=0.05$	$q=0.02$	$q=0$
A	27.7296	110.5046	136.4542	184.1069	290.1801	562.5778
B	3.3029	7.4319	6.9890	7.5105	8.8884	10.9777
C	−0.5393	−5.2859	−4.0250	−4.3550	−5.8356	−8.1040
D	0.4872	2.2885	1.6073	1.6630	2.1836	2.9843
$N=200$	$q=0.4$	$q=0.2$	$q=0.1$	$q=0.05$	$q=0.025$	$q=0$
A	26.0305	61.3858	175.6926	231.8540	253.1515	381.0905
B	3.5741	5.2719	8.5271	8.9492	8.9831	10.2157
C	−1.0107	−2.2387	−5.9740	−6.1313	−6.0314	−7.3571
D	0.7723	1.0023	2.4076	2.3712	2.2990	2.7650
$N=400$	0.4	0.2	0.1	0.05	0.025	0
A	20.7042	61.4690	144.1771	231.8540	244.6135	337.8036
B	2.6497	5.8002	8.2783	8.9492	9.4590	10.4022
C	0.5391	−3.1303	−5.8618	−6.1313	−6.8720	−7.8835
D	0.0284	1.4343	2.4076	2.4257	2.7008	3.0578

the equilibrium depletant density distribution. The functional Ω is related to the intrinsic Helmholtz free-energy functional $\mathcal{F}$ via [42]

$$\Omega[\rho] = \mathcal{F}[\rho] + \int \mathrm{d}^3x \rho(\mathbf{x};\mathbf{r})[V_{\mathrm{ext}}(\mathbf{x};\mathbf{r}) - \mu_{\mathrm{p}}], \quad (6)$$

where μ_{p} is the polymer chemical potential and $V_{\mathrm{ext}}(\mathbf{x};\mathbf{r})$ is the external field due to the interaction of the depletants with the two colloids fixed at the origin and at $\mathbf{r}$, i.e., $V_{\mathrm{ext}}(\mathbf{x};\mathbf{r}) = V_{\mathrm{cp}}(x) + V_{\mathrm{cp}}(|\mathbf{x}-\mathbf{r}|)$.

The intrinsic Helmholtz free-energy functional can be separated into ideal and excess parts,

$$\mathcal{F}[\rho] = \mathcal{F}_{\mathrm{id}}[\rho] + \mathcal{F}_{\mathrm{ex}}[\rho], \quad (7)$$

with the ideal functional known exactly,

$$\beta\mathcal{F}_{\mathrm{id}}[\rho] = \int \mathrm{d}^3x \rho(\mathbf{x};\mathbf{r})\{\ln[\Lambda^3\rho(\mathbf{x};\mathbf{r})] - 1\}, \quad (8)$$

where Λ is the thermal de Broglie wavelength. For the excess free-energy functional, we adopt the accurate mean-field approximation [19,43,44],

$$\mathcal{F}_{\mathrm{ex}}[\rho] = \frac{1}{2}\iint \mathrm{d}^3x\mathrm{d}^3y V_{\mathrm{pp}}(|\mathbf{x}-\mathbf{y}|)\rho(\mathbf{x};\mathbf{r})\rho(\mathbf{y};\mathbf{r}), \quad (9)$$

with the aforementioned polymer-polymer effective interaction $V_{\mathrm{pp}}(|\mathbf{x}-\mathbf{y}|)$. Minimization of the grand potential of Eq. (6) yields the following self-consistent equation that must be satisfied by the equilibrium polymer density profile $\rho(\mathbf{x};\mathbf{r})$ [45]:

$$\rho(\mathbf{x};\mathbf{r}) = \rho_{\mathrm{b}} \exp\{-\beta[V_{\mathrm{cp}}(x) + V_{\mathrm{cp}}(|\mathbf{x}-\mathbf{r}|)]\} \times \exp\left[-\beta\int \mathrm{d}^3y V_{\mathrm{pp}}(|\mathbf{x}-\mathbf{y}|)\Delta\rho(\mathbf{y};\mathbf{r})\right], \quad (10)$$

where ρ_{b} is the bulk (reservoir) depletant density and $\Delta\rho(\mathbf{y};\mathbf{r}) = \rho(\mathbf{y};\mathbf{r}) - \rho_{\mathrm{b}}$, and we have made use of the expressions (8) and (9) to eliminate the chemical potential μ_{p} in its favor.

We solve Eq. (10) iteratively using the Picard method [46]. To take advantage of the cylindrical symmetry of the problem, the anisotropic solvent density profile is constructed on a two-dimensional (x,θ) grid, and the convolution integrals in

TABLE VI. Fitting parameters for the linear polymer-colloid effective interactions of Eq. (3), for chains of different length N and size ratio q.

$N=100$	$q=0.55$	$q=0.27$	$q=0.14$	$q=0.07$	$q=0.03$	$q=0$
A	9.6326	16.7853	47.3336	100.3501	127.6363	257.4591
B	2.2111	2.6467	5.5166	7.6988	8.1193	10.4432
C	0.8020	0.79538	−1.8298	−4.1411	−4.3554	−7.0097
D	0	0	0.5233	1.3061	1.3068	2.2703
$N=200$	$q=0.55$	$q=0.28$	$q=0.14$	$q=0.07$	$q=0.03$	$q=0$
A	8.8096	15.8193	39.3081	79.3428	131.0893	182.7135
B	2.1758	2.8247	5.2146	7.3117	8.9291	9.8255
C	0.8547	0.6113	−1.4961	−3.7854	−5.6307	−6.5441
D	0	0	0.4037	1.1956	1.8662	2.1667
$N=400$	$q=0.55$	$q=0.28$	$q=0.14$	$q=0.07$	$q=0.03$	$q=0$
A	8.6941	15.5247	37.7861	81.0460	107.9754	133.7678
B	2.2760	2.9310	5.3447	7.8608	8.5346	8.9159
C	0.8026	0.5434	−1.7084	−4.7236	−5.2741	−5.4873
D	0	0	0.4971	1.6418	1.7659	1.7733

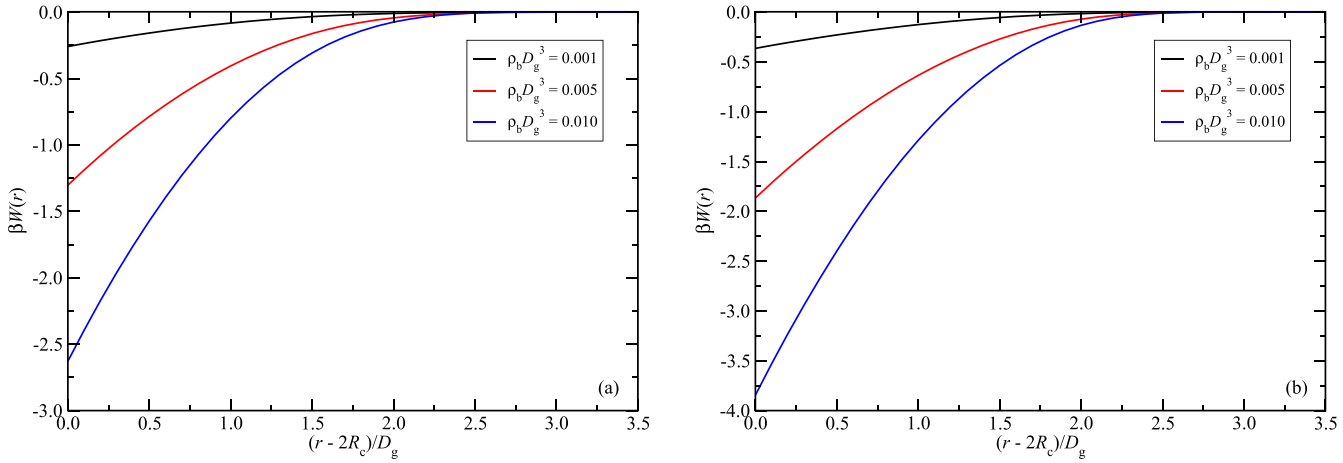

FIG. 9. The depletion potentials $\beta W(r)$ between two colloids of radius R_c, induced by polymers with different bulk (reservoir) densities $\rho_b D_g^3$, as indicated in the legends. (a) Linear chains with size ratio $q = 0.03$; (b) ring polymers with size ratio $q = 0.025$. The horizontal axis expresses the surface-to-surface distance between the two colloids, $r - 2R_c$, in units of the polymer's diameter of gyration D_g.

Eq. (7) are performed by expanding the corresponding functions in Legendre polynomials [47]. We found that using 200 polynomials was sufficient to obtain converged results. The step size along the radial coordinate of the grid was taken to be $0.05R_g$, and the total number of points along this coordinate was taken to be 500. The tolerance criterion for terminating the iterative Picard procedure was set to 10^{-5}.

The magnitude of the depletant-induced mean force $F_d(r)$ on the colloidal particle at the origin with the second colloid fixed at $\mathbf{r}$ that can be obtained is [48]

$$F_d(r) = -\int d^3x\, \rho(\mathbf{x};\mathbf{r})\, \nabla V_{cp}(x) \cdot \hat{\mathbf{r}}, \tag{11}$$

with the unit vector $\hat{\mathbf{r}} = \mathbf{r}/r$, and the depletion interaction $W(r)$ between the two colloids is given by the relation [49]

$$W(r) = \int_r^\infty F_d(r')dr'. \tag{12}$$

Examples of the resulting depletion potentials are shown in Fig. 9, where it can be seen that the ring polymers result in much stronger attractions than linear ones for fixed values of the size ratio q and the reservoir polymer density $\rho_b D_g^3$, where D_g denotes the diameter of gyration of the polymers.

The stronger depletion effect of ring polymers in comparison with linear ones for fixed values of R_g and c/c^* can be rationalized as follows. Consider some value of R_g, fixed for both linear and ring polymers, as well as a solution of either type, which contains N_p macromolecules of degree of polymerization N in the macroscopic volume V. The polymer density $\rho = N_p/V$ and the monomer concentration $c = N_p N/V$ are obviously related via $c = N\rho$. The overlap density ρ^* is the density for which the whole volume is filled with nonoverlapping polymers and, omitting a constant $3/(4\pi)$ of the order of unity, it can be expressed as

$$\rho^* = R_g^{-3}. \tag{13}$$

It is also clear that fractions of polymer densities or monomer concentrations over their overlap values coincide,

$$\rho/\rho^* = c/c^*. \tag{14}$$

Now, let $\beta V_{pp}(r)$ be the effective interaction between two linear or between two ring polymers at separation r between their centers of mass. In the coarse-grained approach that we employ, in which every polymer has been rendered into a soft colloid of size R_g, this interaction takes the form

$$\beta V_{pp}(r) = \Phi_i(r/R_g), \tag{15}$$

where $i \in \{\text{linear}, \text{ring}\}$. The two dimensionless functions $\Phi_i(x)$ of the dimensionless argument x are shown in Fig. 7 and it is evident that the (soft) repulsion between rings is stronger than that between linear chains. Accordingly, by considering the integral over the interactions,

$$\tilde{\Phi}_i(k=0) = 4\pi \int_0^\infty x^2 \Phi_i(x)dx, \tag{16}$$

we immediately establish that

$$\tilde{\Phi}_{\text{ring}}(k=0) > \tilde{\Phi}_{\text{linear}}(k=0). \tag{17}$$

To be quantitative, using the data for the $N = 400$ polymers, we obtain $\tilde{\Phi}_{\text{ring}}(k=0) \cong 44$ and $\tilde{\Phi}_{\text{linear}}(k=0) \cong 16$.

To calculate the osmotic pressure of an interacting polymer solution at any density ρ, we employ the accurate mean-field approximation for the Helmholtz free-energy functional $\beta F[\rho]$ given by Eqs. (8) and (9), which, for a uniform system, results in

$$\frac{\beta F_i(\rho)}{N_p} = \ln\left(\rho R_g^3\right) + \frac{N_p}{2V} R_g^3 \tilde{\Phi}_i(k=0) + 3\ln\left(\frac{\Lambda}{R_g}\right) - 1. \tag{18}$$

The osmotic pressure $\beta\Pi_i$ results from Eq. (18) above as $\beta\Pi_i = -\partial(\beta F_i)/\partial V$; multiplying with R_g^3 to render the quantity dimensionless and using Eqs. (13) and (14) above, we obtain

$$\beta R_g^3 \Pi_i(c/c^*) = \frac{c}{c^*} + \frac{1}{2}\left(\frac{c}{c^*}\right)^2 \tilde{\Phi}_i(k=0). \tag{19}$$

The last equation, together with inequality (17) above, prove that for a fixed value of R_g, the osmotic pressure of the ring solution exceeds that of the linear one at any common value

of the ratio c/c^* of the two solutions,

$$\Pi_{\text{ring}}(c/c^*) > \Pi_{\text{linear}}(c/c^*). \tag{20}$$

We note that the ideal contribution to the osmotic pressure is identical in both cases and it is only the effective polymer-polymer interactions that cause deviations, which are quadratic in c/c^*. It is thus precisely these interactions that enhance the depletion action of the rings, and all effects due to the ring architecture are encoded into a single, effective quantity. We consider this to be, at the same time, a nontrivial and surprising effect, allowing us to capture a lot of information regarding the polymers' architecture in a single parameter.

VI. PHASE BEHAVIOR

To calculate the phase diagram, we follow the standard approach [9,48] and we map the two-component colloid-polymer mixture onto an effective one-component colloidal system by tracing out the polymeric component. This goal is accomplished via Eq. (5), whereby the bare hard-sphere colloid-colloid potential $V_{\text{cc}}(r)$ is augmented by the polymer-mediated depletion interaction $W(r)$ obtained from Eq. (12) using the DFT formalism outlined above. In calculating the phase diagram, we consider both fluid (vapor and liquid) and solid phases. The phase boundaries are obtained by equating the pressure and the colloid chemical potential in the two coexisting phases [9,48]. The pressure P_{f} of the fluid phase is given by [9]

$$\beta P_{\text{f}} v_{\text{c}} = \frac{\phi_{\text{c}} + \phi_{\text{c}}^2 + \phi_{\text{c}}^3 - \phi_{\text{c}}^4}{(1-\phi_{\text{c}}^3)} + \frac{\rho_{\text{c}}\phi_{\text{c}}}{2}\int \mathrm{d}^3 r \beta W(r), \tag{21}$$

where $v_c = 4\pi R_{\text{c}}^3/3$ is the volume of the colloidal sphere, ρ_{c} is the colloid number density, and $\phi_{\text{c}} = \rho_{\text{c}} v_{\text{c}}$ is the colloid packing fraction. The first term on the right-hand side of Eq. (21) originates from the Carnahan-Starling equation of state [50], while the second term comes from the mean-field treatment of the effective colloid-colloid attraction due to the polymer-mediated depletion interaction. The chemical potential μ_{f} of the fluid phase is given by [9]

$$\beta\mu_{\text{f}} = \ln\phi_{\text{c}} + \frac{3-\phi_{\text{c}}}{1-\phi_{\text{c}}^3} - 3 + \rho_{\text{c}}\int \mathrm{d}^3 r \beta W(r). \tag{22}$$

For the fcc solid, the pressure P_{s} is given by [9]

$$\beta P_{\text{s}} v_{\text{c}} = \frac{3\phi_{\text{c}}\phi_{\text{cp}}}{\phi_{\text{cp}} - \phi_{\text{c}}} + \frac{\rho_{\text{c}}\phi_{\text{c}}}{2}\int \mathrm{d}^3 r \beta W(r), \tag{23}$$

where $\phi_{\text{cp}} = \pi/(3\sqrt{2})$ is the value of ϕ_{c} at close packing. Finally, the chemical potential μ_{s} of the solid is given by [9]

$$\beta\mu_{\text{s}} = 3\ln\left[\frac{3\phi_{\text{c}}}{2(\phi_{\text{cp}} - \phi_{\text{c}})}\right] + \frac{3\phi_{\text{cp}}}{\phi_{\text{cp}} - \phi_{\text{c}}} + \rho_{\text{c}}\int \mathrm{d}^3 r \beta W(r). \tag{24}$$

By imposing the conditions of the equality of pressure and chemical potential in the two coexisting phases, one obtains the two respective colloid packing fractions at coexistence. Note that $W(r)$ depends on the reservoir depletant density ρ_{b}; the transformation to the system representation is achieved via $c = \rho_{\text{b}}(1-\phi_{\text{c}})$ [9].

In Fig. 10, we show representative results for the resulting phase diagrams or colloid-ring polymer and colloid-linear

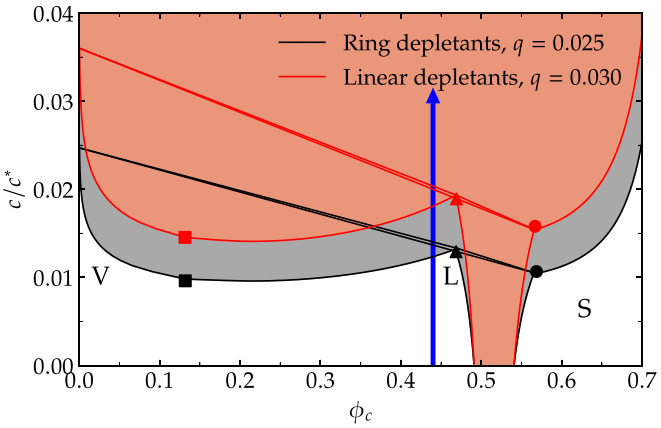

FIG. 10. Representative theoretical phase diagrams obtained by the approach described in the text for a colloid-ring mixture (black lines) and a colloid-linear mixture (red lines) of similar size ratio. The gray- (red-)shaded regions denote phase coexistence between the pure phases in the white area below (for the linear depletants, part of that white area appears gray as it is occupied by the phase-coexistence region of the colloid-ring mixtures). The pure phases are the colloidal fcc crystal (S), the colloidal liquid (L), and the colloidal vapor (V). The think black (red) lines denote the three-phase triangle between the V, L, and S at the triple points, and the black (red) square the critical point. The filled triangle and circle denote the location of the L and S phases at triple coexistence with the V phase, for which $\phi_{\text{c}} \cong 0$. The vertical blue line represents a path of fixed colloid packing fraction $\phi_{\text{c}} = 0.44$, as in the experiments.

polymer mixtures for size ratios $q = 0.025$ (ring depletants) and $q = 0.030$ (linear depletants), which also lie very close to the experimental parameters of the samples Ring-50 and Linear-10, respectively, presented in Table II. Both depletants induce a demixing transition between a colloidal liquid (L) and a colloidal vapor (V), as well as a subsequent phase separation into vapor and polymer-poor colloidal crystal (S) upon increasing the polymer concentration at fixed colloid packing fraction ϕ_{c}. Our theoretical approach yields an equilibrium phase diagram, whereas in the experiments, we probed the onset of colloidal gelation. Gelation and crystallization, however, are strongly correlated in colloid-polymer mixtures, as shown, e.g., in Refs. [34,51], where it was established that gels are found in the regions of the phase diagram slightly above the onset of the fluid-crystal coexistence. In conjunction with Fig. 10, we see that for the $q = 0.025$ colloid-ring mixture and at $\phi_{\text{c}} = 0.44$, theory locates the onset of gelation at $(c/c^*)_{\text{gel}} \approx 0.020$, which compares well with the finding $(c/c^*)_{\text{gel}} \approx 0.039$ from experiments; see Fig. 5. Moreover, theory predicts that for approximately the same value of the size ratio q, the ring polymers induce solidification (and thus gelation) at a lower value of c/c^* than their linear counterparts, in agreement with experiments. In theory, the value of $(c/c^*)_{\text{gel}}$ for the linear chains exceeds that of the rings by a factor $\approx$1.5, whereas in the experiment (main plot of Fig. 5), this is much larger. However, the theoretical calculation is based on the assumption that both the linear chains and the rings are long and flexible, a condition not fulfilled for the Linear-10 sample in our experiments. For the Ring-160/Linear-73 combination, which satisfies this assumption,

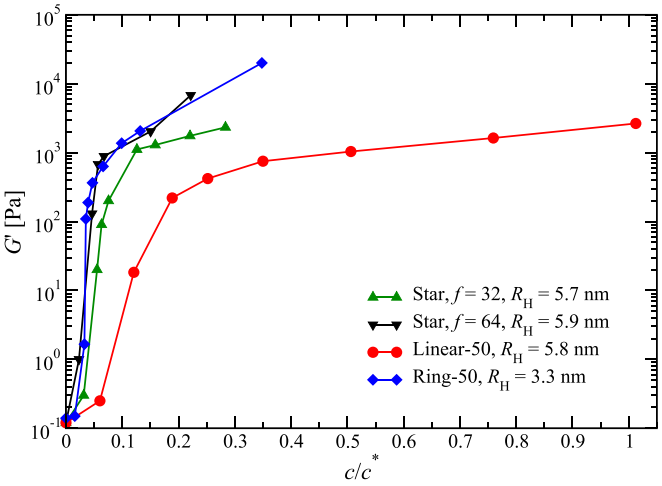

FIG. 11. Comparison of depleting efficiency of polymers with different architecture. Same conditions as in Fig. 5.

the ratio of $(c/c^*)_{\rm gel}$ between linear and ring depletants is indeed ≈2, as can be seen in the inset of Fig. 5.

VII. CONCLUSIONS

By combining rheological experiments with computer simulations, coarse-graining techniques, and theoretical approaches based on density functional theory, we have shown that rings polymers induce much stronger cohesion through depletion on colloidal particles than their linear counterparts of the same size and chemistry. This demonstrates the dramatic effect that polymer architecture has on tuning the structure and dynamics of hard colloids, and hence the properties of the gel through entropic changes only, adding to an existing and growing body of knowledge regarding the effects of polymer topology on the rheology of pure polymer solutions and melts [52,53]. Future perspectives include the investigations of the effects of polymer rigidity and charge on the rheology of colloid-cyclic polymer mixtures, to take advantage of readily available technologies in employing rigid DNA minirings as additives in colloidal suspensions.

ACKNOWLEDGMENTS

We thank A. B. Schofield and G. Petekidis for providing the PMMA particles, and R. A. Farimani for technical assistance. S.A.E. acknowledges financial support from the Erwin Schrödinger International Institute for Mathematics and Physics (ESI) as a Senior Research Fellow. We acknowledge support by a FORTH synergy grant (RINGS) and from the European Union (Horizon-MSCA-Doctoral Networks) through the project QLUSTER (HORIZON-MSCA-2021-DN-01-GA101072964). The computational results presented here have been achieved using the Vienna Scientific Cluster (VSC).

APPENDIX: STAR POLYMERS AS DEPLETING AGENTS

In a star polymer, the interactions can be fine tuned by adjusting the number of arms, f. Here, we choose two polystyrene star polymers of the same size, but with two different functionalities, $f = 32$ and $f = 64$, which were synthesized by means of anionic polymerization using high vacuum techniques and chlorosilane linking chemistry [54]. In particular, each arm has molar mass $M_w^{(a)} = 8$ kg/mol, resulting in total molar masses $M_w = 256$ kg/mol for $f = 32$ and $M_w = 512$ kg/mol for $f = 64$. The hydrodynamic radii are $R_{\rm H} = 5.7$ nm and $R_{\rm H} = 5.9$ nm, and the overlap concentrations are $c^* = 0.548$ g/ml and $c^* = 1.318$ g/ml for the $f = 32$ star and the $f = 64$ star, respectively. Polydispersity was kept <1.15; see Table I. As shown in Fig. 11, stars create a stronger gel compared to linear chains of the same size. A star polymer with higher f is "harder" [35], featuring stronger star-star and star-colloid repulsions, and yields a stronger gel. Notably, the star with $f = 64$ behaves similarly to the ring with the smaller size. Based on these findings, we anticipate that a star polymer with high functionality (e.g., $f \geqslant 64$) and the same size as the ring makes a stronger gel.

[1] P. Bolhuis and D. Frenkel, Prediction of an expanded-to-condensed transition in colloidal crystals, Phys. Rev. Lett. **72**, 2211 (1994).
[2] A. Stradner, H. Sedgwick, F. Cardinaux, W. C. K. Poon, S. U. Egelhaaf, and P. Schurtenberger, Equilibrium cluster formation in concentrated protein solutions and colloids, Nature (London) **432**, 492 (2004).
[3] F. Sciortino, S. Mossa, E. Zaccarelli, and P. Tartaglia, Equilibrium cluster phases and low-density arrested disordered states: The role of short-range attraction and long-range repulsion, Phys. Rev. Lett. **93**, 055701 (2004).
[4] A. I. Campbell, V. J. Anderson, J. S. van Duijneveldt, and P. Bartlett, Dynamical arrest in attractive colloids: The effect of long-range repulsion, Phys. Rev. Lett. **94**, 208301 (2005).
[5] K. Dawson, G. Foffi, M. Fuchs, W. Götze, F. Sciortino, M. Sperl, P. Tartaglia, T. Voigtmann, and E. Zaccarelli, Higher-order glass-transition singularities in colloidal systems with attractive interactions, Phys. Rev. E **63**, 011401 (2000).
[6] K. N. Pham, A. M. Puertas, J. Bergenholtz, S. U. Egelhaaf, A. Moussaïd, P. N. Pusey, A. B. Schofield, M. E. Cates, M. Fuchs, and W. C. K. Poon, Multiple glassy states in a simple model system, Science **296**, 104 (2002).
[7] F. Sciortino, P. Tartaglia, and E. Zaccarelli, Evidence of a higher-order singularity in dense short-ranged attractive colloids, Phys. Rev. Lett. **91**, 268301 (2003).
[8] E. Zaccarelli, Colloidal gels: Equilibrium and nonequilibrium routes, J. Phys.: Condens. Matter **19**, 323101 (2007).
[9] H. Lekkerkerker and R. Tuinier, *Colloids and the Depletion Interaction* (Springer, Berlin, 2011), Vol. 833.
[10] W. C. K. Poon, The physics of a model colloid-polymer mixture, J. Phys.: Condens. Matter **14**, R859 (2002).
[11] A. Kulkarni and C. Zukoski, Depletion interactions and protein crystallization, J. Cryst. Growth **232**, 156 (2001).
[12] P. N. Pusey, in *Les Houches, Session LI, Liquids, Freezing, and the Glass Transition*, edited by J. Hansen, D. Levesque, and J. Zinn-Justin (North-Holland, Amsterdam, 1991).

[13] S. Asakura and F. Oosawa, On Interaction between two bodies immersed in a solution of macromolecules, J. Chem. Phys. **22**, 1255 (1954).

[14] S. Asakura and F. Oosawa, Interaction between particles suspended in solutions of macromolecules, J. Polym. Sci. **33**, 183 (1958).

[15] A. Imhof and J. K. G. Dhont, Experimental phase diagram of a binary colloidal hard-sphere mixture with a large size ratio, Phys. Rev. Lett. **75**, 1662 (1995).

[16] B. Lonetti, M. Camargo, J. Stellbrink, C. N. Likos, E. Zaccarelli, L. Willner, P. Lindner, and D. Richter, Ultrasoft colloid-polymer mixtures: Structure and phase diagram, Phys. Rev. Lett. **106**, 228301 (2011).

[17] D. Truzzolillo, D. Marzi, J. Marakis, B. Capone, M. Camargo, A. Munam, F. Moingeon, M. Gauthier, C. N. Likos, and D. Vlassopoulos, Glassy states in asymmetric mixtures of soft and hard colloids, Phys. Rev. Lett. **111**, 208301 (2013).

[18] S. Darvishi, M. A. Nazeer, M. Tyagi, Q. Zhang, S. Narayanan, S. Kizilel, and E. Senses, Nonlinear architectures can alter the dynamics of polymer–nanoparticle composites, Macromolecules **54**, 10118 (2021).

[19] I. Chubak, E. Locatelli, and C. N. Likos, Ring polymers are much stronger depleting agents than linear ones, Mol. Phys. **116**, 2911 (2018).

[20] I. Chubak, C. N. Likos, and S. A. Egorov, Multiscale approaches for confined ring polymer solutions, J. Phys. Chem. B **125**, 4910 (2021).

[21] S. F. Tead, E. J. Kramer, G. Hadziioannou, M. Antonietti, H. Sillescu, P. Lutz, and C. Strazielle, Polymer topology and diffusion: A comparison of diffusion in linear and cyclic macromolecules, Macromolecules **25**, 3942 (1992).

[22] G. B. McKenna, G. Hadziioannou, P. Lutz, G. Hild, C. Strazielle, C. Straupe, P. Rempp, and A. J. Kovacs, Dilute solution characterization of cyclic polystyrene molecules and their zero-shear viscosity in the melt, Macromolecules **20**, 498 (1987).

[23] Y. Jeong, Y. Jin, T. Chang, F. Uhlik, and J. Roovers, Intrinsic viscosity of cyclic polystyrene, Macromolecules **50**, 7770 (2017).

[24] D. Cho, S. Park, K. Kwon, T. Chang, and J. Roovers, Structural characterization of ring polysterene by liquid chromatography at the critical condition and the MALDI-TOF mass spectrometry, Macromolecules **34**, 7570 (2001).

[25] H. C. Lee, H. Lee, W. Lee, T. Chang, and J. Roovers, Fractionation of cyclic polystyrene from linear precursor by HPLC at the chromatographic critical condition, Macromolecules **33**, 8119 (2000).

[26] M. Lee, M. Alcoutlabi, J. J. Magda, M. J. Solomon, X. Shi, and G. B. McKenna, The effect of the shear-thickening transition of model colloidal spheres on the sign of N_1 and on the radial pressure profile in torsional shear flows, J. Rheol. **50**, 293 (2006).

[27] T. Solomon and M. J. Solomon, Stacking fault structure in shear-induced colloidal crystallization, J. Chem. Phys. **124**, 134905 (2006).

[28] L. T. Shereda, R. G. Larson, and M. J. Solomon, Local stress control of spatiotemporal ordering of colloidal crystals in complex flows, Phys. Rev. Lett. **101**, 038301 (2008).

[29] P. Ballesta, N. Koumakis, R. Besseling, W. Poon, and G. Petekidis, Slip of gels in colloid–polymer mixtures under shear, Soft Matter **9**, 3237 (2013).

[30] M. Laurati, S. U. Egelhaaf, and G. Petekidis, Nonlinear rheology of colloidal gels with intermediate volume fraction, J. Rheol. **55**, 673 (2011).

[31] H. Henning Winter and F. Chambon, Analysis of linear viscoelasticity of a crosslinking polymer at the gel point, J. Rheol. **30**, 367 (1986).

[32] A. Zaccone, H. Wu, and E. DelGado, Elasticity of arrested short-ranged attractive colloids: Homogeneous and heterogeneous glasses, Phys. Rev. Lett. **103**, 208301 (2009).

[33] M. Laurati, G. Petekidis, N. Koumakis, F. Cardinaux, A. B. Schofield, J. M. Brader, M. Fuchs, and S. U. Egelhaaf, Structure, dynamics, and rheology of colloid-polymer mixtures: From liquids to gels, J. Chem. Phys. **130**, 134907 (2009).

[34] J. Bergenholtz, W. C. K. Poon, and M. Fuchs, Gelation in model colloid-polymer mixtures, Langmuir **19**, 4493 (2003).

[35] C. N. Likos, H. Löwen, M. Watzlawek, B. Abbas, O. Jucknischke, J. Allgaier, and D. Richter, Star polymers viewed as ultrasoft colloidal particles, Phys. Rev. Lett. **80**, 4450 (1998).

[36] N. Koumakis and G. Petekidis, Two step yielding in attractive colloids: Transition from gels to attractive glasses, Soft Matter **7**, 2456 (2011).

[37] E. Fillipidi, T. R. Cristiani, C. D. Eisenbach, J. H. Waite, J. N. Israelachvili, B. Kollbe Ahn, and M. T. Valentine, Toughening elastomers using mussel-inspired iron-catechol complexes, Science **358**, 502 (2017).

[38] I. Chubak, C. N. Likos, and J. Smrek, Topological and threading effects in polydisperse ring polymer solutions, Mol. Phys. **119**, e1883140 (2021).

[39] A. Narros, A. J. Moreno, and C. N. Likos, Architecture-induced size asymmetry and effective interactions of ring polymers: Simulation and theory, Macromolecules **46**, 9437 (2013).

[40] P. G. Bolhuis, A. A. Louis, J. P. Hansen, and E. J. Meijer, Accurate effective pair potentials for polymer solutions, J. Chem. Phys. **114**, 4296 (2001).

[41] P. G. Bolhuis and A. A. Louis, How to derive and parameterize effective potentials in colloid polymer mixtures, Macromolecules **35**, 1860 (2002).

[42] R. Evans, The nature of the liquid-vapour interface and other topics in the statistical mechanics of nonuniform, classical fluids, Adv. Phys. **28**, 143 (1979).

[43] A. A. Louis, P. G. Bolhuis, and J. P. Hansen, Mean-field fluid behavior of the Gaussian core model, Phys. Rev. E **62**, 7961 (2000).

[44] A. Lang, C. N. Likos, M. Watzlawek, and H. Löwen, Fluid and solid phases of the Gaussian core model, J. Phys.: Condens. Matter **12**, 5087 (2000).

[45] A. J. Archer and R. Evans, Solvent-mediated interactions and solvation close to fluid-fluid phase separation: A density functional treatment, J. Chem. Phys. **118**, 9726 (2003).

[46] S. A. Egorov and K. Binder, Effect of solvent quality on the dispersibilty of polymer-grafted spherical nanoparticles in polymer solutions, J. Chem. Phys. **137**, 094901 (2012).

[47] N. Patel and S. A. Egorov, Interactions between nanocolloidal particles in polymer solutions: Effect of attractive interactions, J. Chem. Phys. **123**, 144916 (2005).

[48] J. Dzubiella, C. N. Likos, and H. Löwen, Phase behavior and structure of star-polymer–colloid mixtures, J. Chem. Phys. **116**, 9518 (2002).

[49] P. Attard, Spherically inhomogeneous fluids. II. Hard sphere solute in a hard-sphere solvent, J. Chem. Phys. **91**, 3083 (1989).

[50] N. F. Carnahan and K. E. Starling, Equation of state for nonattracting rigid spheres, J. Chem. Phys. **51**, 635 (1969).

[51] W. C. K. Poon, J. S. Selfe, M. B. Robertson, S. M. Ilett, A. D. Pirie, and P. N. Pusey, An experimental study of a model colloid-polymer mixture, J. Phys. II France **3**, 1075 (1993).

[52] M. Kapnistos, M. Lang, D. Vlassopoulos, W. Pyckhout-Hintzen, D. Richter, D. Cho, T. Chang, and M. Rubinstein, Unexpected power-law stress relaxation of entangled ring polymers, Nat. Mater. **7**, 997 (2008).

[53] M. Tu, O. Davydovich, B. Mei, P. K. Singh, G. S. Grest, K. S. Schweizer, T. C. O'Connor, and C. M. Schroeder, Unexpected slow relaxation dynamics in pure ring polymers arise from intermolecular interactions, ACS Polym. Au **3**, 307 (2023).

[54] J. Roovers, L. L. Zhou, P. M. Toporowski, M. Vanderzwan, H. Iatrou, and N. Hadjichristidis, Regular star polymers with 64 and 128 arms. Models for polymeric micelles, Macromolecules **26**, 4324 (1993).